Applied Clay Science 250 (2024) 107269

Contents lists available at ScienceDirect

Applied Clay Science

journal homepage: www.elsevier.com/locate/clay

Research Paper

Detection limits of kaolinites and some common minerals in binary mixtures by short-wave infrared spectroscopy

Ángel Santamaría-López [a,*], Mercedes Suárez [a], Emilia García-Romero [b,c]

[a] Departamento de Geología, Universidad de Salamanca, Plaza de la Merced s/n, 37008 Salamanca, Spain
[b] Departamento de Mineralogía y Petrología, Universidad Complutense de Madrid, José Antonio Novais 12, 28040 Madrid, Spain
[c] Instituto de Geociencias (IGEO), Universidad Complutense de Madrid – Consejo Superior de Investigaciones Científicas, Doctor Severo Ochoa 7, 28040 Madrid, Spain

ARTICLE INFO

Keywords:
Kaolinites
Mineral identification
Mineral quantification
SWIR spectroscopy

ABSTRACT

The identification of minerals is key for adequately characterizing geological materials at different scales, from the study of outcrop surfaces to extraplanetary exploration. One of the most widely used identification methodologies in recent years is the spectroscopy in the visible, near infrared and short-wave infrared wavelength ranges (VNIR-SWIR spectroscopy). In polymineralic samples the position, geometry and intensity of the absorption features are parameters that can depart from the single-mineral samples as interference phenomena occur between the spectra of each mineral present. In this work it was studied and compared the reflectance spectra of binary mixtures to determine the detection limits of each mineral. For that, binary mixtures of well crystallized kaolinite and poorly crystallized kaolinite mixed with calcite, dolomite, gypsum, quartz and feldspar were prepared. The selected minerals are common in the Earth's crust in different geological contexts, mainly in sedimentary environments, in as alterations associated with ore deposits, and they have also been described on the surface of several extraterrestrial terrains. Binary samples spectra, their continuum removed-spectra and their second derivatives were compared, and identification limits, expressed as a percentage of each mineral, were obtained. These identification limits vary depending on the minerals mixed and the normalization method applied. The results after continuum removal showed that the identification of both kaolinites, in mixtures with calcite and dolomite, is possible if its content is ≥5%; and ≥15%, in mixtures with gypsum. The content to identify calcite must be ≥75%; whereas for dolomite is ≥60%; and ≥20% for gypsum. The implementation of the second derivative entailed some variations in the previous identification limits. Thus, kaolinite is identifiable if its content is ≥5% in all the mixtures; whereas carbonates have identification limits of 90%; and 5% in the case of gypsum. The identification of kaolinite in the presence of both tectosilicates is relatively easy (only 5% content is necessary regardless of the normalization method used). These limits were obtained from a constrained strategy based only in the study of binary mixtures, and easily obtained determination parameters. In that sense, they will probably diverge from the limits obtained in real cases, as other factors such as the number of constituent minerals, grain size, homogenization, and/or crystallinity, among others, may influence the identification. However, the results offer a diagnosis, based on a systematic study, of the arising issues to identify different minerals in polymineralic samples in laboratory or by remote sensing approaches. It is particularly notable the high detection limits of both carbonates in the presence of kaolinite. Therefore, it highlights the ease with which a misidentification of important constituents can occur in SWIR spectroscopy.

1. Introduction

The visible, near infrared, and short-wave infrared (VNIR-SWIR) spectroscopy is one of the most powerful, faster, and non-invasive technique used for mineralogical studies. Consequently, spectroradiometric studies in this wavenumber interval, at different spatial scales, are done for the exploration of ore minerals (e.g., Ramanaidou and Wells, 2015; Dill, 2016), ore-waste ratio determinations (e.g., Desta and Buxton, 2020) or other geological studies since the last decades of the XX Century. These studies comprise both laboratory and field work, including the acquisition and analysis of point spectra to the acquisition and analysis of images obtained by remote sensing (e.g., Bishop et al.,

* Corresponding author.
E-mail address: a.santamaria@usal.es (Á. Santamaría-López).

https://doi.org/10.1016/j.clay.2024.107269
Received 7 November 2023; Received in revised form 19 January 2024; Accepted 21 January 2024
Available online 29 January 2024

2017), mainly satellite and airborne images.

VNIR-SWIR spectroscopy operates in the wavelength range between 350 nm and 2500 nm, and as it is well known, most rock-forming minerals such as hydrated silicates including clay minerals, sulphates, and carbonates, among others have characteristic absorption features in this wavenumber region that can be consulted in different spectral libraries or in seminal papers such as those of Hunt (1977), Clark and Roush (1984) and Bishop et al. (2008), among others.

However, in natural materials, involving several components, the identification of the existing minerals prove to be more changeling than in single-mineral samples (Sunshine et al., 1990; Haest et al., 2012; Mulder et al., 2013; Gomez et al., 2015; Gomez et al., 2018; Bishop, 2019). The main difficulty lies in the overlapping of different absorption bands in closer regions of the spectrum (Robertson et al., 2016). Because of that, the geometry of the spectrum of the polymineralic sample deviates from the theoretical spectrum of the existing minerals, as changes in the position and morphology of the initial absorption bands, their possible disappearance and/or variations in the global reflectance of the spectrum can occur (Clark, 1999; Mulder et al., 2013). For example, in mixtures with several different clay minerals the identification of smectite and illite may be limited by the presence of kaolinite (e.g., Simpson and Rae, 2018). Additionally, lower mineral abundance leads to a decrease in the intensity of its characteristic absorption bands, so its fingerprint in the polymineralic sample-spectrum may be overshadowed by minerals with higher proportions, but also with more dominant absorption bands (Clark, 1999; Bishop, 2019). Several procedures and preprocessing techniques have been applied in order to easy the identification of minerals in polymineralic samples by comparing with spectral libraries (Clark et al., 2003; Flahaut et al., 2012; Mulder et al., 2013; Tiecher et al., 2021). Some methodologies have been tested to carry out quantifications including Modified Gaussian Modeling (MGM) (Sunshine et al., 1990; Sunshine and Pieters, 1993; Bishop et al., 2011; Rialland et al., 2021), Exponential Gaussian Optimisation (EGO) (Pompilio et al., 2009) and the Radiative Transfer Models (RTMs) carried out by Shkuratov et al. (1999), Hapke (2002) and Shkuratov and Grynko (2005). However, some of the previous methodologies are based on complex mathematical procedures, and therefore other simpler and faster procedures for spectral signals preprocessing are often preferred (in particular, for multiple in situ spectra treatment, obtained by portable acquisition equipments). In this sense, one of the most used and accessible preprocessing methodologies for studying the reflectance spectra is the analysis of its second derivative which improves the resolution of overlapping spectra (Bou-Orm et al., 2020) by revealing weak spectral features and it is used for reliable determining the band centers (Bishop et al., 2002; Madejová et al., 2017). It has been previously used to identify subtle reflectance drops in the absorption features which are hardly visible in the original curve (Demetriades-Shah et al., 1990; Kariuki et al., 2004). Similarly, preprocessing the spectra by continuum removal facilitates comparison between them. Both are widely used normalization methodologies in the literature, which can however present identification challenges if the spectra of polymineralic samples diverge from the spectra of single minerals. In this study, the morphological modifications (both in the raw and normalized spectra) caused when the proportions of different minerals in the sample vary, have been analyzed. To illustrate this, we have determined the mineral detection limits of the SWIR spectroscopy from mixtures of kaolinites and several non-clay minerals (calcite, dolomite, gypsum, quartz and feldspar). The selected minerals are common in the Earth's crust and they have also been described on the surface of several extraterrestrial terrains (e.g., Poulet et al., 2005). Some examples of materials combining the studied non-clay minerals with kaolinites include carbonate-rich mudstones (e.g., Ohiara et al., 2023), lacustrine carbonate rocks, hydrothermal alterations both with carbonates (e.g., Géring et al., 2022; Simpson, 2015), and sulphates (e.g., Çelik et al., 1999; Simpson, 2015), fault rocks, soils (Naimi et al., 2022), carbonate mining wastes (Alayet et al., 2017), among others. Kaolinites and tectosilicates occur commonly associated in various environments and sedimentary rocks.

Kaolinites generally present a lower complexity in their fingerprints compared to other clay minerals (e.g., number and position of absorption features). This makes them good candidates for initial work that addresses the morphological variations of their spectra in the presence of other minerals, and constitutes a starting point for similar future studies based on more structurally complex clay minerals.

2. Metodology

For this study two kaolinites, one well-ordered (Ord-Kaol) and one poorly-ordered (Dis-Kaol) (Kga-1b and Kga-2 respectively; Clay Mineral Repository, described by Chipera and Bish, 2001), were mixed with five different non-clay minerals: calcite (Cal), dolomite (Dol), gypsum (Gp), quartz (Qz) and feldspar (Fsp) (non-clay minerals abbreviations according to Warr, 2021). All minerals were previously pulverized in agate mortar, and subsequently different proportions of them were weighted and mixed in order to prepare binary samples weighing 3 g in total (i.e., kaolinite + non-clay mineral). Samples were mixed to obtain a homogeneous distribution of mineral grains in the mixture. Ten mixtures sets of new samples were obtained from the mixture of Ord-Kaol or Dis-Kaol with each of the non-clay minerals. Each set included nineteen binary samples containing different mineral proportions, with a continuous variation of 5% (from 95% kaolinite – 5% non-clay mineral, 90% kaolinite – 10% non-clay mineral, up to a sample containing 5% kaolinite – 95% non-clay mineral). The samples were labeled as "kaolinite% - non clay mineral%", such as Ord-Kaol 65% - Cal 35%, for instance. Therefore, a total of 7 pure minerals, and 10 mixtures sets, with 19 binary samples each set, were studied. The SWIR spectroscopy analysis of these 197 samples was carried out with a field spectroradiometer ASD FieldSpec 4 Hi-Res which operates in a wavelength range comprising between 350 nm and 2500 nm and it is equipped with a contact probe. The equipment operates with two detectors (SWIR1 and SWIR2) to cover the short-wave range, with 8 nm of spectral resolution. Spectralon© was used as white reference and each final reflectance spectrum is the average of 25 spectra. Samples were prepared in a metallic sample holder and measured in direct contact with the contact probe, protected with glass without response. The resulting spectra were visualized in Spectragryph (version 1.2.15; Menges, 2016) software.

For easing the comparison between binary mixture samples, two different normalization methods were applied to the final spectra: (1) the continuum removal (CR) and (2) the second derivative. The CR preprocessing methodology defines a convex envelope fitted over the top of each spectrum by connecting local maxima. This allows removing the overall shape of the spectrum and provides a common baseline for comparing the resulting continuum removed-spectra (CR-spectra) (Clark and Roush, 1984; Gomez et al., 2008; Lagacherie et al., 2008; Makarewicz et al., 2009). The CR was performed by using a script written in Python which uses the PySptools library (Cardoso-Fernandes et al., 2021). The CR of each binary mixture sample was carried out separately in two delimited regions of its respective spectrum: (1) between 1255 nm and 1690 nm and (2) from 2120 nm to 2260 nm. These regions were selected considering the presence, in the unmixed kaolinites spectra, of two main diagnostic doublets: the first one with bands at ~1395 nm and ~1413 nm; and the second one at ~2165 and ~2208 nm. These doublets are hereinafter referred as ~1400 nm and ~2200 nm doublets respectively. The applying the CR to delimited regions of each spectrum was preferable to carrying it out on the complete SWIR wavelength range. In this way, for each region the script fulfilled a better normalization up to an intensity value of 1, and comparison between binary mixture samples CR-spectra was improved. The output data of the script included the area (S) of the absorption features included in the selected regions of the CR-spectra, in addition to the depth (D) of their main bands (i.e., at 1413 nm and 2208 nm respectively). The script obtains the values of S and D for each single CR-spectrum separately. The S of each absorption feature is defined as the space comprised

between the curve of each single CR-spectrum and a horizontal line fixed at an intensity value of 1 (see Fig. S1). Second derivatives were obtained by ViewSpec Pro (version 6.2) software with a derivative gap settled on 7. Several tests were carried out with different derivative gap values. Lower values than 7 increased the noise ratio, and higher over-smoothed the signal, obstructing the identification of peaks. The height (D_2) of the most remarkable peaks in the resulting second derivatives was measured (from a base line at y = 0) with Spectragryph (version 1.2.15). Additionally, X Ray Diffraction (XRD) patterns (Fig. S2) were obtained with a Bruker diffractometer D8 Advance ECO, with LYNXEYE SSD160 high resolution detector and Cu Kα radiation, operating at 0.05° 2 theta/s. All samples are pure or almost pure, with the exception of feldspar which contains few traces of illite (~1%). Inductively Coupled Plasma (ICP) chemical analyses for kaolinites are included the Supplementary data document.

3. Results and discussion

The spectral response in the VNIR-SWIR wavenumber range of the studied minerals (Fig. S3) is very well known (e.g., Gaffey, 1986; Clark et al., 1990; Delineau et al., 1994; Clark, 1999; Madejová and Komadel, 2001; Cloutis et al., 2006; Cloutis et al., 2010; Madejová et al., 2017; Bishop, 2019; Bishop et al., 2021). The characteristic absorption features of each mineral and their assignations are described in detail the Supplementary data document. The results showed that the spectral behavior of mixtures with Ord-Kaol and Dis-Kaol are, in general, very similar. Because of that, for reasons of simplicity, in the figures of this study it has been opted for showing only the results with the Ord-Kaol. The figures regarding mixtures with Dis-Kaol are included in the Supplementary data document. On the other hand, if notable differences in the results of both kaolinites exist, these are pointed out and discussed through the text. In the following figures, only a selection of mixtures is included for each set (i.e., 90%–10%, 80%–10%, up to 10%–90%). Figures with all samples are in Supplementary data, in addition to figures of mixtures with quartz and feldspar.

3.1. SWIR spectra of the binary mixture samples

The reflectance spectra of the binary mixture samples of Ord-Kaol, calcite, dolomite and gypsum are included in Figs. 1–2. Curves are displayed offset for clarity. The wavelength range in these figures has been limited between 1100 nm and 2500 nm, as the most characteristic

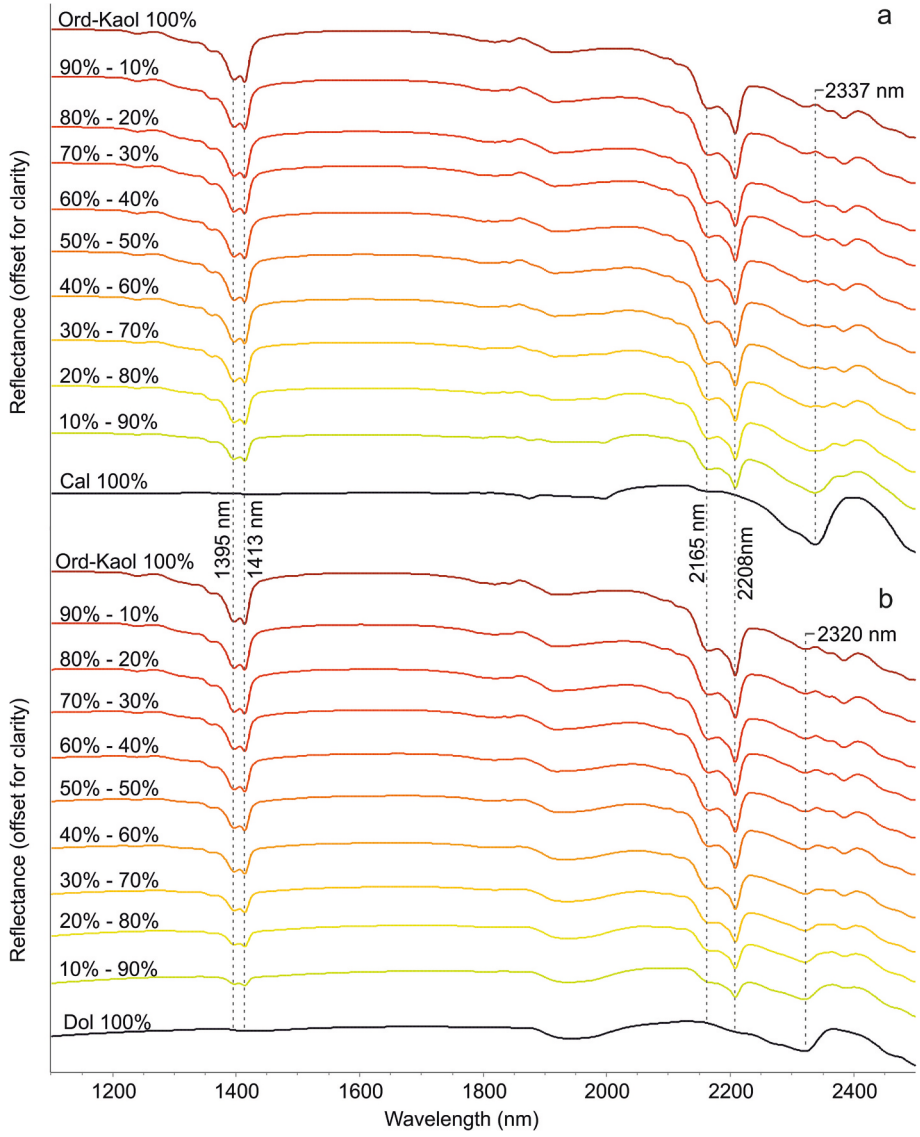

Fig. 1. SWIR spectra of binary mixture samples of well-ordered kaolinite with calcite (Ord-Kaol – Cal) (a), and well-ordered kaolinite with dolomite (Ord-Kaol – Dol) (b). The spectra are offset for clarity.

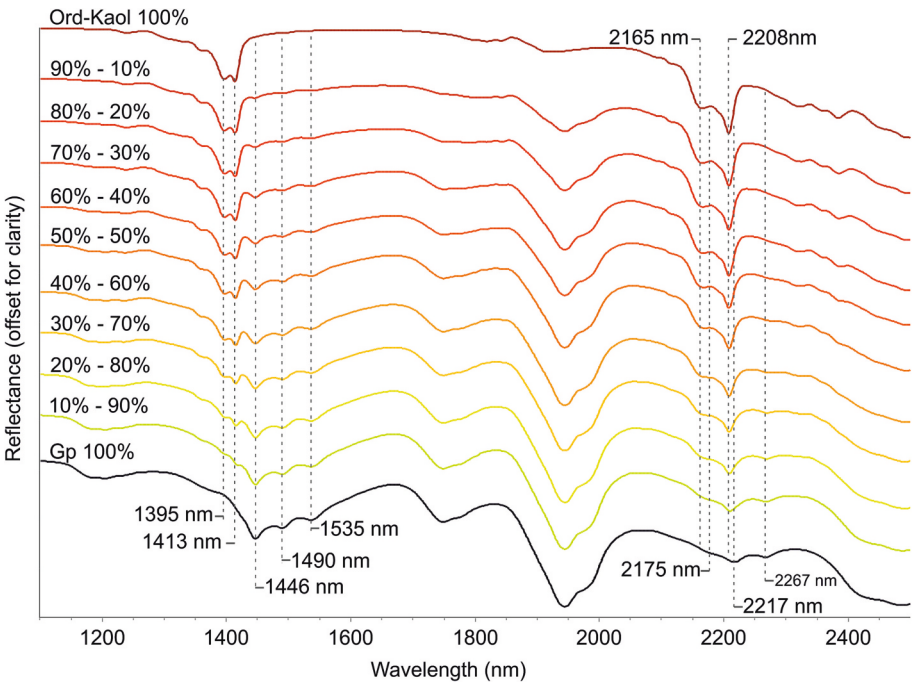

Fig. 2. SWIR spectra of binary mixture samples of well-ordered kaolinite with gypsum (Ord-Kaol – Gp). The spectra are offset for clarity.

absorption features of the minerals studied are display in this field. It is possible to notice the different behavior of each set in a glance related to the differences among the absorption coefficients of each mineral and the overlapping of some features in the sets. In the mixtures of kaolinite and carbonates, the reflectance decreases in the features-lacking regions of the original clay mineral spectra (e.g., between 1600 nm and 1700 nm) as the calcite and dolomite contents are increased (e.g. Fig. S4). In a glance, the depth and area of both studied doublets progressively decreases as the carbonates contents are higher, but in detail, several modifications can be addressed. The behavior of the reflectance value of the kaolinite ~1400 nm doublet can be particularly puzzling as curves tend to overlap (Fig. S4), hampering the determination of a general increasing- or decreasing-trend. But, in general, a reflectance initial reflectance drop followed by increasing arises in all kaolinite-carbonate sets. Despite these modifications both the bands at ~1395 nm and ~1413 nm are mostly preserved in calcite-rich and dolomite-rich samples (Fig. 1). The maximum reflectance in the ~2200 nm doublet initially drops and subsequently increase in all the studied kaolinite-carbonate sets. The band at ~2165 nm of the Ord-Kaol spectrum becomes a shoulder in mixtures with ≥80% of dolomite (Fig. 1b). The interference effects between the spectra of kaolinites and carbonates are complex in those wavelength ranges in which these minerals present absorption features (in agreement with previous studies as Mulder et al., 2013 and Ducasse et al., 2020). The bands at 1875 nm and 1995 nm of calcite, and the broad band in the dolomite spectrum centered at 1940 nm, modify the geometry of the 1913 nm absorption feature observed in both kaolinites. However, it is important to note that this band in the kaolinite spectra reflects the adsorbed water (i.e., not structural water). Therefore, it would not be a constant and reliable diagnostic feature in order to compare different kaolinite samples. The 2337 nm band of calcite has a notable impact on the geometry of the clay mineral spectra at this wavelength, increasing the sharpness of the kaolinites spectra (e.g., see how the right-flank of the 2337 nm band of calcite progressively varies the slope of the Ord-Kaol curve at ~2355 nm; Fig. 1a). The interference of characteristic features of kaolinites and calcite presented here are in line with Ducasse et al. (2020) who reported the disappearance of montmorillonite spectral features when calcite content is ≥80%. Mulder et al. (2013) also described the blurring of kaolinite, smectite and mica features in presence of calcite (and quartz). The 2320 nm feature of the dolomite approximately coincides with the 2323 nm band of the kaolinites, increasing its sharpness as the carbonate content is higher. This last observation is accompanied by a general decrease and subsequent recovery of the reflectance values between 2000 nm and 2500 nm (Fig. S4b). It should be noted that the positions of the kaolinite bands in mixtures with calcite and dolomite do not diverge appreciably from the spectra of pure samples.

The spectra of kaolinites are severely modified as the gypsum content increases, and vice versa (Fig. 2). The same phenomenon is illustrated by Robertson et al. (2016) in spectra obtained from montmorillonite-gypsum binary samples. The sulfate triplets superpose the ~1400 nm doublet (partially) and the ~2200 nm doublet of kaolinites. The sulfate spectral signature progressively mask both kaolinites signature up to finally dominate the binary samples geometry in these regions. The identification of the 1395 nm, 1413 nm and 2165 nm kaolinite bands is particularly hampered as the geometry of these is not preserved as the gypsum content is higher. The kaolinite band at 2208 nm is mostly conserved as it is roughly coupled with the 2217 nm band of gypsum. There is a progressively increase in the binary sample's spectra sharpness at ~1200 nm, 1744 nm and ~ 1944 nm because of gypsum bands. Once again, it should be noted that despite the notable modifications described, the positions of the kaolinite bands do not diverge appreciably from the spectra of pure samples.

The main modification of kaolinite spectrum in mixtures with quartz and feldspar is the general decrease in the global reflectance (e.g., between 1600 nm and 1700 nm) (Figs. S8 and S9) (in agreement with results of Zhang et al., 2001). This is related to the low global reflectance of the tectosilicates spectra, and how both minerals non-specifically absorb the radiation in this interval of wavenumbers. Even though feature-interferences do not occur, the mixture of kaolinite with quartz and feldspar can have a negative impact on its identification (e.g., Mulder et al., 2013) as the doublets fingerprint tend to be attenuated. The small content of illite in the feldspar sample has a limited impact in the identification of kaolinite, as it slightly increases the sharpness in the 1900 nm and 2200 nm regions but does not cause bands displacement. Identification of the band-lacking feldspar is not affected by the illite.

As reported in previous studies (Zhang et al., 2001; Bou-Orm et al.,

2020; Ducasse et al., 2020; McKeown et al., 2011), the spectra of the binary samples are progressively more similar to the starting spectrum of the minerals studied the higher the content of one of them in the mixture, as logical. The spectra of binary samples with approximately equal contents of kaolinite and non-clay mineral (e.g., the Ord-Kaol 50% - Gp 50% sample; Fig. 2) tend to include absorption features characteristic of the spectra of the minerals separately, although with geometrical modifications, in many cases, severe. That is, the spectrum of a mineral mixture is not simply a sum of original absorption features, with unaltered morphologies, but a unique spectral fingerprint.

3.2. CR-spectra of the binary mixture samples

The implementation of CR facilitated the comparison between binary mixtures spectra with different global reflectance (Figs. 3 and 4) and allowed looking for the possible correlation between the minerals proportions and parameters measured in the CR-spectra (D and S). Plots showing each parameter value vs non-clay mineral content are included in Fig. 5. The increment of calcite and dolomite contents leads to a general D and S decreasing of the selected kaolinites absorption features (Fig. 5). A smoothing of the bands at 1395 nm and 2160 nm occurs in these mixtures, but the identification of these kaolinite features is still possible in the spectrum with only 5% kaolinite (Fig. S10 and S11). The

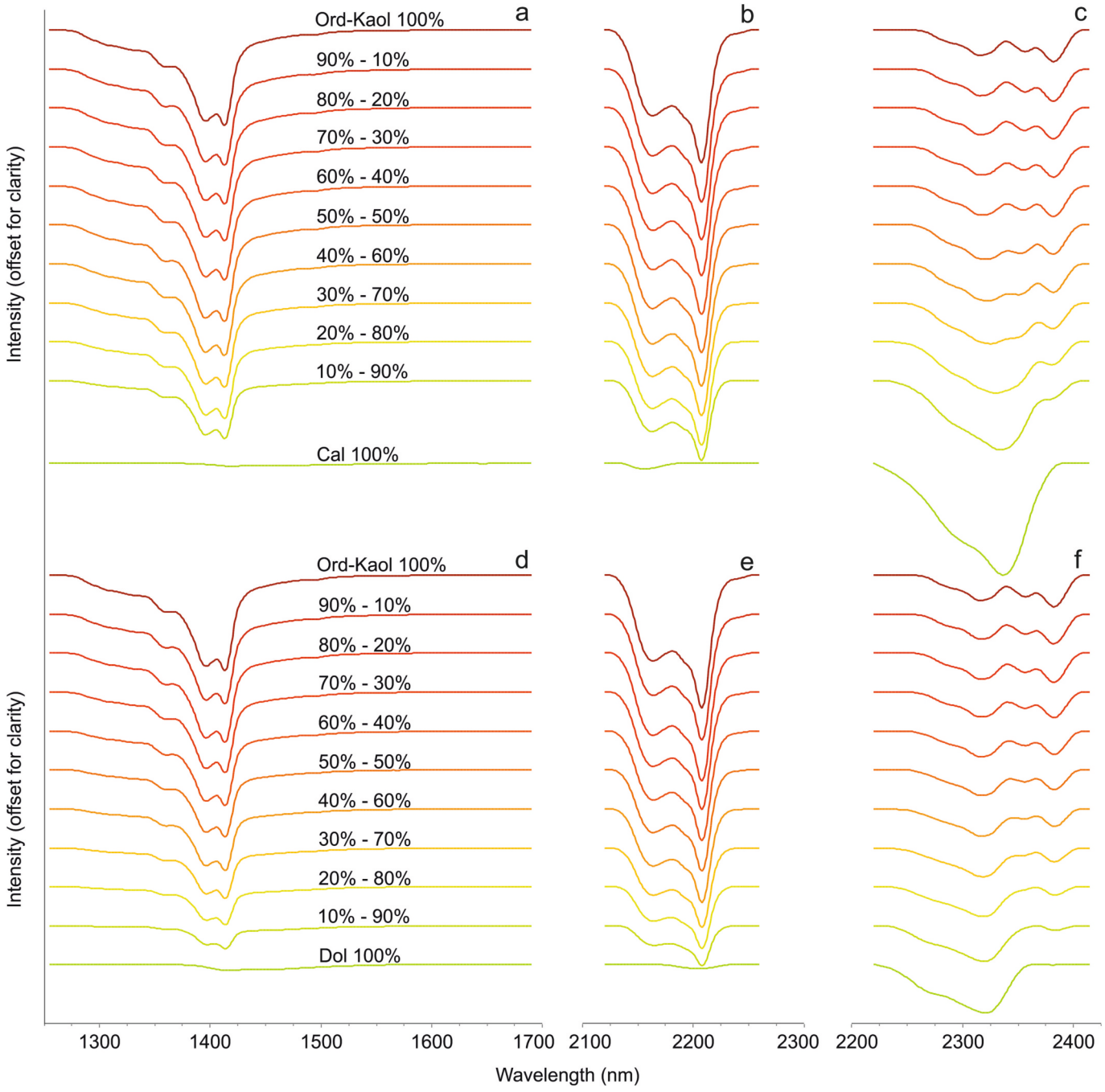

Fig. 3. Continuum removed-spectra regions of binary mixture samples of well-ordered kaolinite with calcite (Ord-Kaol – Cal) (~1400 nm doublet, a; ~2200 nm doublet, b; 2337 nm calcite band; c); and well-ordered kaolinite with dolomite (Ord-Kaol – Dol) (~1400 nm doublet, d; ~2200 nm doublet, e; 2320 nm dolomite band; f). The CR-spectra are offset for clarity.

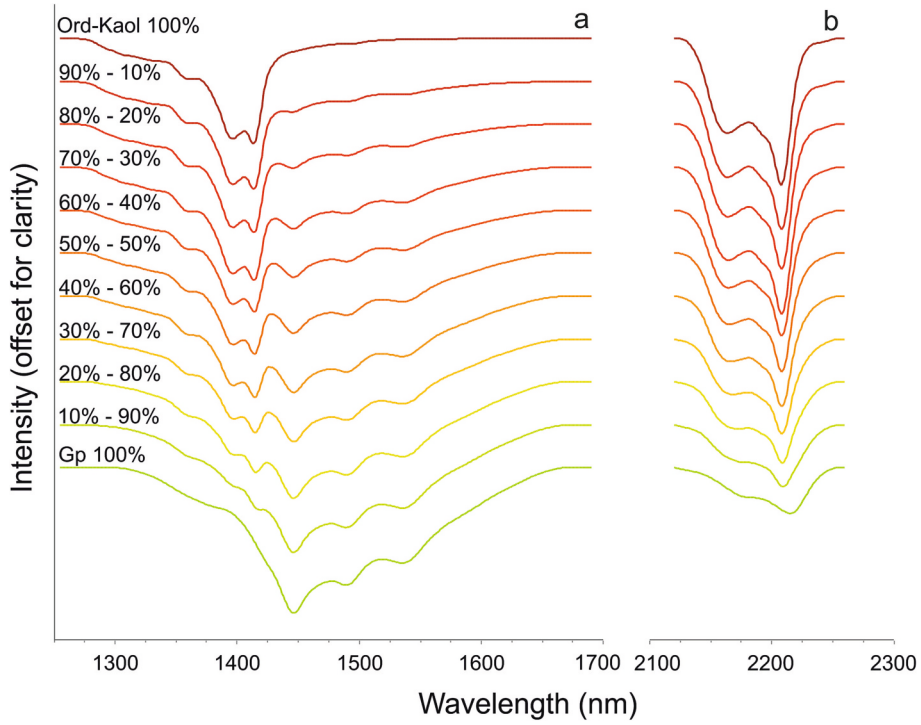

Fig. 4. Continuum removed-spectra regions of binary mixture samples of well-ordered kaolinite with gypsum (Ord-Kaol – Gp) (~1400 nm doublet, a; ~2200 nm doublet, b). The CR-spectra are offset for clarity.

decrease curves of S and D as the content of calcite increases follows a more asymptotic trend (Fig. 5) than the case of the mixtures with other non-clay minerals. This indicates that calcite does not obscure the absorption features of kaolinites as efficiently. This phenomenon is verified in the doublets at 1400 nm and 2200 nm shown in Fig. S10a, b, in which the spectra with the highest-kaolinite – lowest-calcite contents (approximately between 100% to 50% of kaolinite; reddish to green spectra) display more stacked than in mixtures with other non-clay minerals (e.g., with dolomite, Fig. S10d, e). Similar spectra-stacking effects were reported by Ducasse et al. (2020) in montmorillonite – non-clay mineral mixtures. Ultimately, the studied clay minerals would be successfully identifiable even in high-calcite samples and terrains. To show the impact of the kaolinites spectra on the carbonates spectra, an additional wavelength region (from 2220 nm to 2415 nm) were included in the Fig. 3c, f. Alayet et al. (2017) demonstrated that carbonates CR-features in this region allowed their identification in presence of kaolinite and gypsum. However, in our opinion the following modifications reduce their reliability. The most prominent calcite band, at 2337 nm, suffers an attenuation as the kaolinite content increases along with a shift towards lower wavelengths (in agreement with Mulder et al. (2013) results on kaolinite-calcite mixtures). Thus, in the samples with ≥25–30% of kaolinite the calcite band cannot be clearly identified, since the convexity-concavity of the curve at ~2337 nm is progressively inverted (Fig. 3c). The identification of the dolomite based on its characteristic band at 2320 nm is also complex because it roughly coincides with a small absorption feature of the kaolinites in that area (Fig. 3f). The spectra of the mixtures with ≥40% kaolinite chaotically overlap, making a robust distinction between the dolomite and kaolinite bands impossible in these samples (Fig. S10f). Other methodologies could improve this identification limits of carbonates in the presence of kaolinite. For example, Hubbard et al. (2024) carried out the identification of calcite, dolomite and montmorillonite (25%, 25% and 50% respectively), and calcite and montmorillonite (80% and 20%), in mixtures of these minerals from treatments based on algorithms characterization applied to normalized spectra with continuum removal.

The increase in the gypsum content leads to an important variation in the CR-spectra of the clay minerals (Fig. 4). With the increase in the sulphate, an initial slight increase in D occurs in the doublets of both kaolinites; followed by a decrease. The S values in the region between 1255 and 1690 nm (Fig. 4a) increases as the progressively larger gypsum triplet combines with the kaolinite doublet (Fig. 5c). In the samples with kaolinite content ≤15% the 1395 nm, 1413 nm and 2165 nm kaolinite bands are severely modified, compromising the clay mineral identification. There is a slight blurring of the bands at 1395 nm and 2165 nm that evolve from well-defined bands to shoulders (Fig. 4). Whereas the 1413 nm band progressively disappears, while shifting towards longer wavelengths (up to 2 nm), due to its proximity to the gypsum 1446 nm band (Fig. 4a). The band at 2208 nm, on the other hand, hardly varies in position (despite being partially overlapped with that of 2217 nm of gypsum) and is distinguishable even in the spectra with lower kaolinite contents (Fig. 4b). Accordingly, it can be considered as a key band for the identification of these clay minerals in mixtures with gypsum. The increment in both quartz and feldspar contents decrease the D and S values of the kaolinite absorption features displayed in the selected regions (Figs. 5, S14, S15 and S16).

The fit of trendlines shown in Fig. 5 and Fig. S16 is generally quite good (R^2 values ranges between 0.89 and 0.99; 26 of a total of 40 trends correspond to $R^2 = 0.99$). The sets with lower R^2 values are mixtures with calcite (R^2 values ranging between 0.89 and 0.95), which are also those that display more asymptotic trends. The equations of these trendlines can be potentially used to quantify the proportion (in %) of the non-clay mineral (i.e., the variable "x" in the equation) and, indirectly, the % of the kaolinite, in each set of mixtures from measured D or S values. However, this approach should be taken with caution since the calculated trendlines can obviously differ between sets with different mixed minerals (e.g., Mathian et al., 2018). For example, although very similar, the trendlines of the Ord-Kaol – Cal and Dis-Kaol – Cal mixtures sets are not strictly identical (Figs. 5 and S16), implying that the type of kaolinite used for each mixture impact differently on their corresponding equations. In samples with gypsum this methodology is even less suitable as the overlapping of bands prevents monitoring the band variation of each endmember separately.

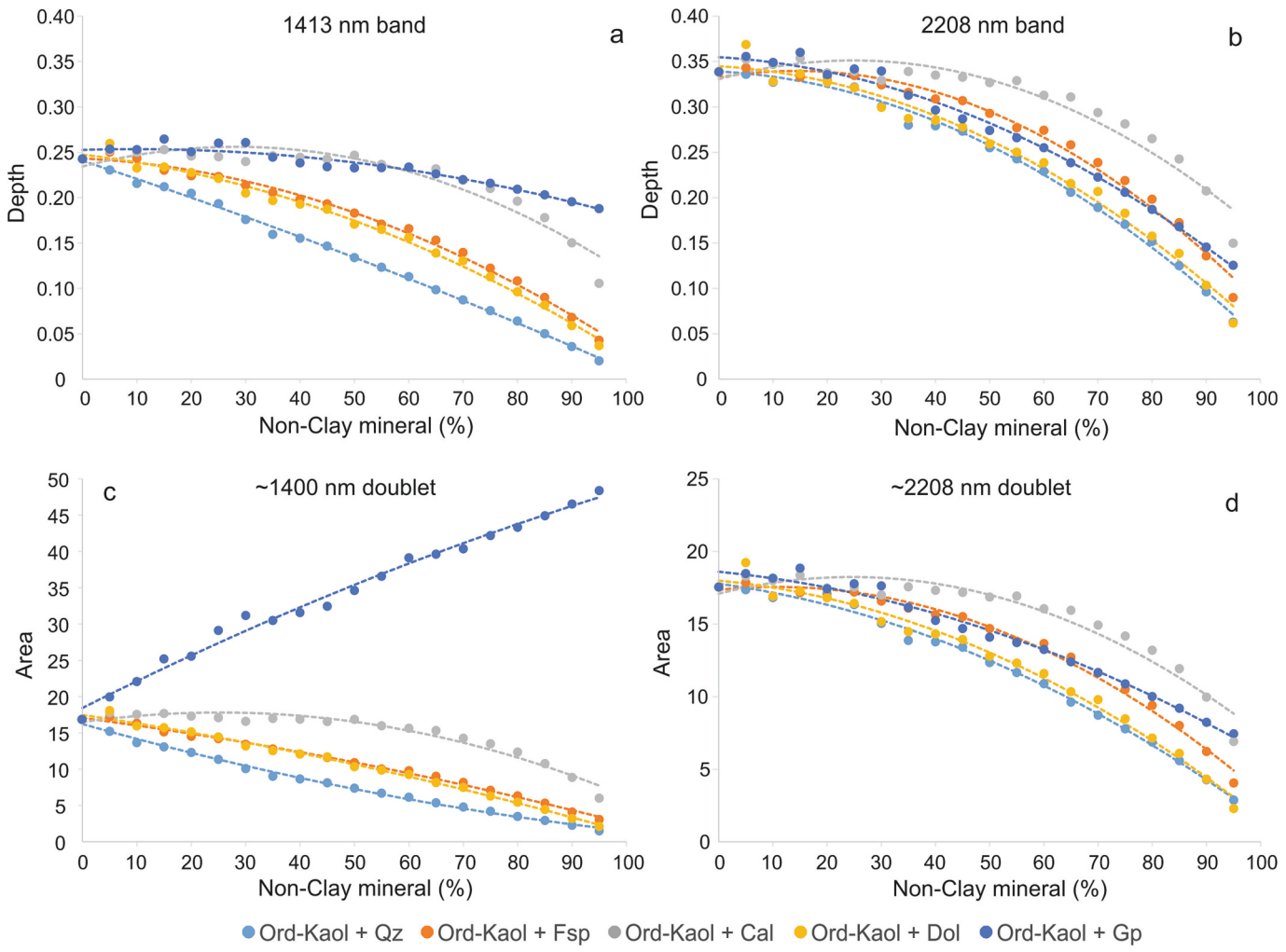

Fig. 5. Diagrams showing the variation of depth and area of characteristic well-ordered kaolinite (Ord-Kaol) bands and doublets respectively vs. the content in non-clay minerals in the binary mixture samples. These parameters were measured in the continuum removed-spectra. (a) 1413 nm band depth; (b) 2208 nm band depth; (c) ~1400 nm doublet area; (d) ~2200 nm doublet area. All the diagrams include the 2nd order polynomial trendlines (dashed lines). Non-clay mineral abbreviations: calcite, Cal; dolomite, Dol; gypsum, Gp; quartz, Qz; and feldspar, Fsp.

3.3. Second derivative of binary mixture samples spectra

The second derivatives of the mixtures sets are included in Figs. 6–7. The D_2 vs non-clay mineral content diagrams are shown in Fig. 8. In general terms, the second derivative of Ord-Kaol and Dis-Kaol spectra are similar between them (e.g., Figs. S17 and S18). However, some differences could be used to distinguish between the two kaolinites. Most of the Ord-Kaol peaks have higher D_2 values. The D_2 difference between the peaks at 1395 nm and 1415 nm is smaller in the Ord-Kaol. Two negative peaks are recognized at 1372 nm and 1381 nm in the Ord-Kaol; and one single peak in the Dis-Kaol. Finally, in the Dis-Kaol a doublet at 1854–1868 nm is better defined.

The use of the second derivatives improves the identification of the kaolinites in the prepared mixtures, compared to the unmodified spectra or CR-spectra. First, the second derivative highlights the presence of the existing features in the original curves. This is particularly important in order to prevent shoulders to be overlooked, or their position misassigned. For example, several shoulders or small bands of the Ord-Kaol CR-spectrum (at ~1308 nm, ~1359 nm, ~1494 nm) (e.g., Fig. 3a) are displayed as peaks in the second derivative (e.g., Fig. 6a). Likewise, the shoulder at 1413 nm in the CR-spectrum of Ord-Kaol 5% - Gp 95% (Fig. S12a) is distinguishable as a peak after applying the second derivative (Fig. 7a). Second, the peaks in the second derivative of a particular spectrum usually display separated, highlighting their presence. For example, the main bands in the ~1400 nm doublet are clearly separated in two different peaks in the second derivative (at ~1395 nm and ~1415 nm, e.g., Fig. 6a). Finally, the peaks of the second derivatives pertaining to the same set tend to be fixed position-stacked, and possible drifting between peaks from different samples are minimized (no >2 nm). This is a valuable improvement to compare the binary samples included in the same set.

Generally, as the content of non-clay minerals in the mixtures increases, the D_2 of the peaks of both kaolinites decreases (Figs. 6–7; S17-S22). Despite the decrease on D_2 these are identifiable even in samples with only 5% kaolinite abundance. The fit of the trend lines shown in Fig. 8 and Fig. S23 is considerably good (R^2 values range between 0.85 and 0.99; 27 of a total of 40 trends present an $R^2 = 0.99$). Trends are exponential in mixtures with dolomite, gypsum, quartz and feldspar. Implying the opaqueness of the kaolinites-fingerprint is manifested even with non-clay mineral low proportions. The asymptotic nature in trends with calcite is more pronounced (Fig. 8). This indicates that the impact of calcite on the D_2 of kaolinite peaks is only noticeable with higher calcite abundances (approximately if calcite content is ≥65–70%).

The dentification of calcite and dolomite surprisingly does not improve after the implementation of the second derivative. Several second derivative peaks of calcite occur in the region between 2220 nm and 2415 nm (2317 nm, 2343 nm, 2365 nm and 2384 nm; Fig. 6c). However, they are quickly deformed by those of the kaolinites

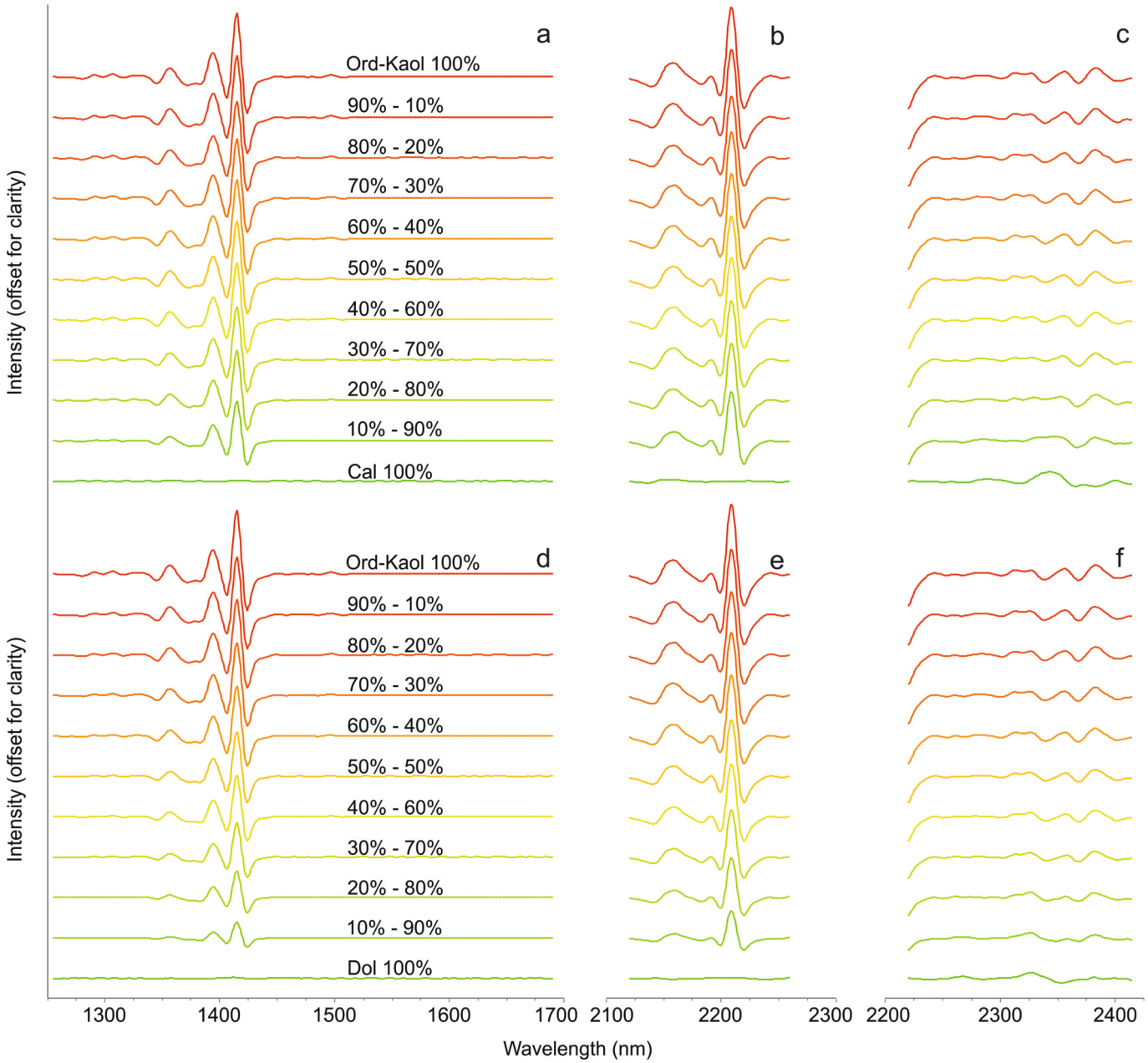

Fig. 6. Second derivative of spectra regions of binary mixture samples of well-ordered kaolinite with calcite (Ord-Kaol – Cal) (a-c); and well-ordered kaolinite with dolomite (Ord-Kaol – Dol) (d-f). The second derivatives are offset for clarity.

(convexity changes usually occur), making calcite identification impossible if the kaolinite content is ≥10%. In the same region, the second derivative peaks of dolomite (e.g., 2267 nm, 2285 nm and 2353 nm; Fig. 6f) are either modified by those of kaolinites or coincide with them and therefore the assignment is confusing (e.g., at 2327 nm and 2381 nm) (Fig. 6f). In general, the identification of dolomite is not reliable with a kaolinite content ≥10%. Several second derivative peaks of gypsum (including 1445 nm, 1458 nm, 1477, 1491, 1507, 1539 nm; Fig. 7) were used to identify this mineral, and it can be detected in samples with only 5% content. Lacking characteristic absorption features, and therefore second derivative peaks, neither quartz nor feldspar can be identified.

3.4. Mineral identification limits

In previous Sections 3.1, 3.2, and 3.3, the arising challenges in the identification of mineral phases in the studied binary mixture samples have been presented, and how two types of normalization processes (CR and second derivative) can be used to minimize these difficulties and to improve results. Even with these preprocesses, the identification of individual minerals can incur a degree of subjectivity and imprecision. Logically, identifying minerals in a mixture depends on whether one or several characteristic absorption features (or second derivative peaks) are present and that these, in addition, show a morphology and position that largely coincides with those expected from that mineral. In this study the obtained detection limits are expressed as the minimum content values (%) of a certain mineral necessary to identify its presence in a mixture (Table 1). Since the absorption coefficients are different for each mineral, the detection limits of each of them depend on the mineral with which it is mixed. For example, based on the CR-data at least 5% of Ord-Kaol is necessary to identify this clay mineral in a mixture with calcite (Table 1). It is important to note, however, that 5% is a limit that may

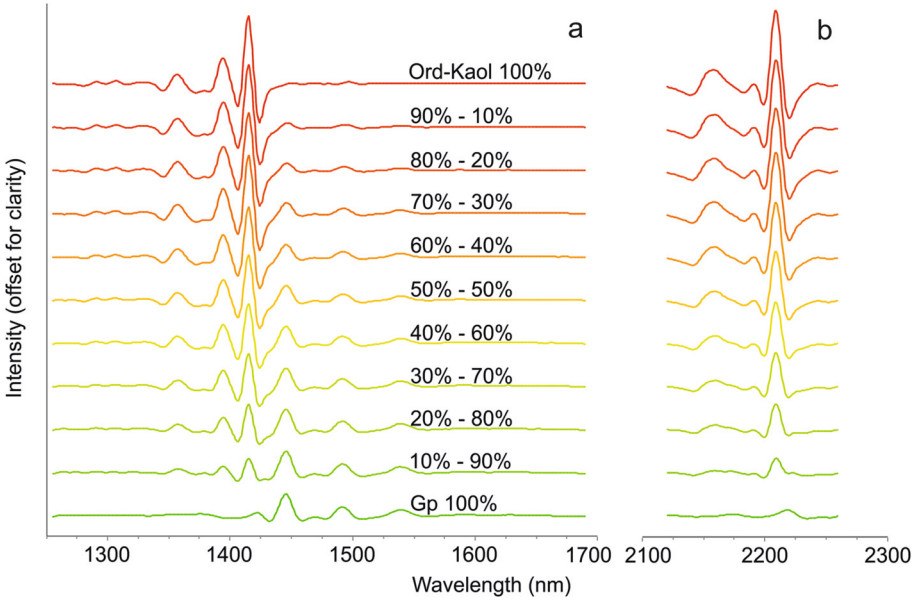

Fig. 7. Second derivative of spectra regions of binary mixture samples of well-ordered kaolinite with gypsum (Ord-Kaol – Gp). The second derivatives are offset for clarity.

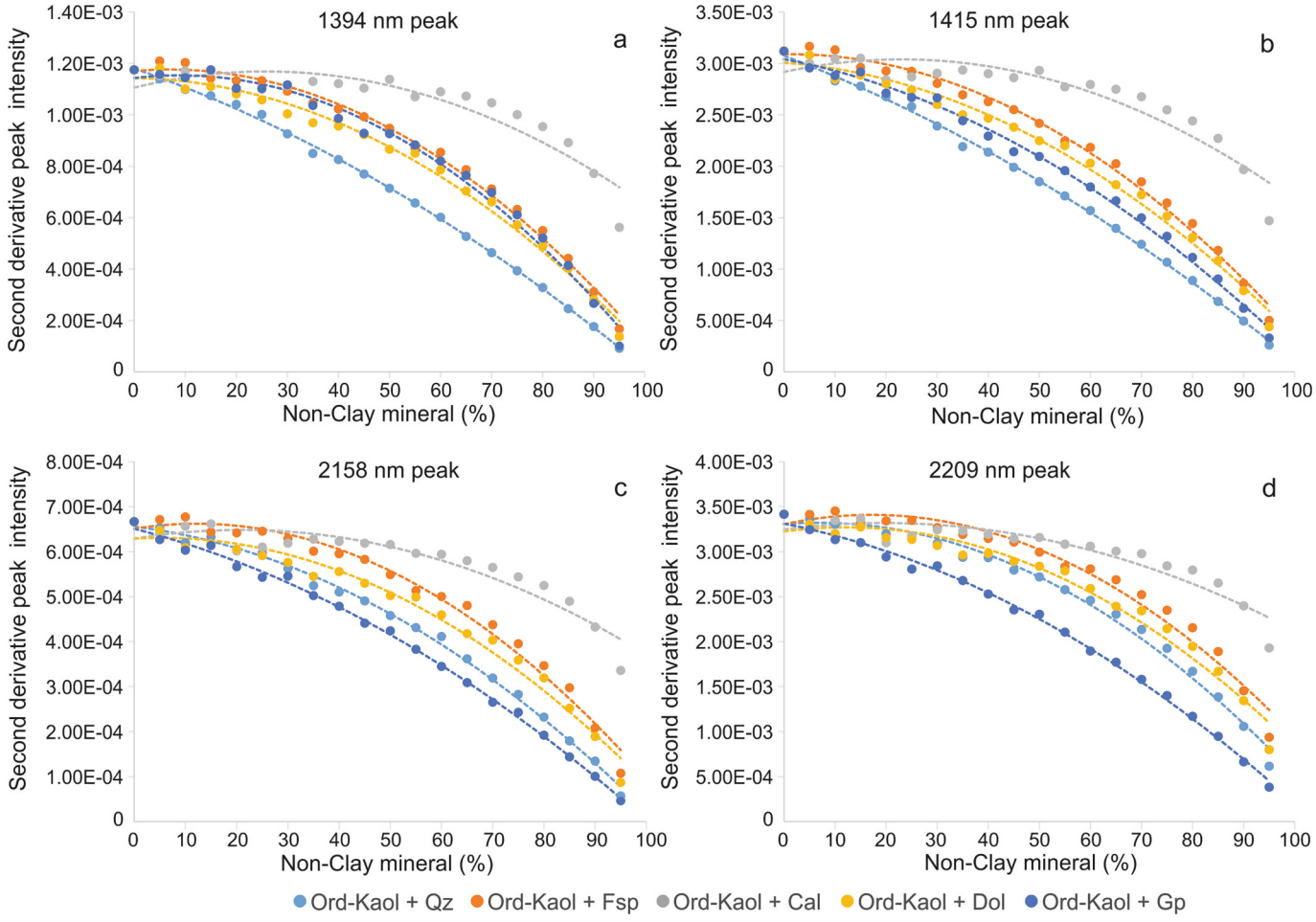

Fig. 8. Diagrams showing the variation of the characteristic well-ordered kaolinite (Ord-Kaol) second derivative peaks depth vs the content in non-clay minerals. (a) 1394 nm peak depth; (b) 1415 nm peak depth; (c) 2158 nm peak depth; (d) 2209 nm peak depth. All the diagrams include the 2nd order polynomial trendlines (dashed lines). Non-clay mineral abbreviations: calcite, Cal; dolomite, Dol; gypsum, Gp; quartz, Qz; and feldspar, Fsp..

Table 1
Well-ordered kaolinite (Ord-Kaol), poorly-ordered kaolinite (Dis-Kaol) and non-clay minerals (calcite, Cal; dolomite, Dol; gypsum, Gp; quartz, Qz; feldspar, Fsp) detection limits in the binary mixtures sets. Each value corresponds to the minimum content (%) of each mineral necessary for allowing its identification from the spectra sets after continuum removal and second derivative. "NI" means it is not possible to identify the mineral in the mixtures.

			Continuum removal	Second derivative
Mixture sets	Ord-Kaol - Cal	Ord-Kaol	5	5
		Cal	75	90
	Dis-Kaol - Cal	Dis-Kaol	5	5
		Cal	75	90
	Ord-Kaol - Dol	Ord-Kaol	5	5
		Dol	60	90
	Dis-Kaol - Dol	Dis-Kaol	5	5
		Dol	60	90
	Ord-Kaol - Gp	Ord-Kaol	15	5
		Gp	20	5
	Dis-Kaol - Gp	Dis-Kaol	15	5
		Gp	20	5
	Ord-Kaol - Qz	Ord-Kaol	5	5
		Qz	NI	NI
	Dis-Kaol - Qz	Dis-Kaol	5	5
		Qz	NI	NI
	Ord-Kaol - Fsp	Ord-Kaol	5	5
		Fsp	NI	NI
	Dis-Kaol - Fsp	Dis-Kaol	5	5
		Fsp	NI	NI

not be strictly real, but exclusively experimental, since it is the minimum proportion of each mineral in the samples prepared for this study. Therefore, the detection limit in a real sample can be even lower. In this study some key-absorption features (i.e., doublets in kaolinites, triplets in gypsum, etc.) and second derivative peaks have been addressed for each mineral. To confirm the presence of a mineral in the prepared binary samples, we consider features must be clearly distinguishable, and largely retain their position. In this regard, it has been considered that these shoulders are equally characteristic of each mineral. This is an approach which assumes the best-case scenario, in which the shoulders can be correctly identified and assigned to each mineral. If this were not the case, the detection limits for kaolinites presented in Table 1 would be higher (i.e., minerals would be more difficult to identify).

Different detection limits have not been determined between binary samples with Ord-Kaol or Dis-Kaol. The two kaolinites studied are relatively easy to identify in the mixtures as the absorption features and second derivative peaks are mostly visible even in binary samples with low clay mineral content. After CR is applied, a kaolinite content of at least 5% is necessary to identify this clay mineral in mixtures with calcite, dolomite, quartz and feldspar; and 15% with gypsum. The CR-preprocessing of the original spectra does not unsure the identification of calcite, dolomite and gypsum as the detection limits are 75%, 60% and 20% respectively. With the second derivatives the kaolinites and gypsum detection limits values are 5%. This improvement in detection after the implementation of the second derivative is in line with the results of Mathian et al. (2018) who established detection limits from binary mixtures of muscovite, talc and Fe-Mg chlorite with kaolinite in lateritic saprolites (obtaining limits ranging between 5% and 10%). Both these phyllosilicates and gypsum present important absorption features whose presence is enhanced by the second derivative. Surprisingly, the implementation of the second derivatives does not improve the detection capacity of carbonates, which however require a content of at least 90% to be clearly identified. Carbonate limits could be improved as demonstrated by Pilorget and Fernando (2021) on nontronite-magnesite mixtures and inversion models based on a Monte Carlo Markov Chains (MCMC) scheme. Quartz and feldspar characteristic absorption features lacking prevents their identification regardless the normalization method applied (Table 1). This is an analytical problem long discussed (e.g., Hubbard et al., 2024) whose solution generally requires the use of techniques that cover longer infrared wavelengths (mid-infrared, MIR) in which features belonging to these minerals can be identified.

It must be considered that in the case of polymineralic natural samples the identification limits determined in this study can, and most probably will, be different. Several factors, in addition to the content and optical properties of the minerals present, may influence the detection in natural samples. The first, logically, is the number of constituents. In this sense, it is reasonable to conclude that a larger number of constituents implies a more complex interaction between individual spectra. Other factors are the homogenization and distribution of the constituents in the natural sample, grain size, the organic matter content, the porosity, compaction, water content, the degree of alteration of the minerals, their crystallinity, etc. (e.g., Crowley, 1986; García-Rivas et al., 2018). In this sense, Pilorget and Fernando (2021) studied, the impact on the identification of several minerals in mixtures based on the grain size of the constituents and their absorbance. They verified that in mixtures of nontronite with magnesite, the former can be successfully quantified, except when the diameter is below a few tens of microns or its proportion is lower than 10%; while the identification of magnesite is considerably less straightforward, particularly if the grain size is fine. The degree of crystallinity of the kaolinite, on the other hand, can condition the spectral curves (e.g., this study), deviating from the standards (e.g., Mathian et al., 2018). This is something that must be considered in certain environments, such as lateritic soils.

4. Conclusions

In this study, binary mixtures of kaolinites with other common non-clay minerals have been carried out in order to determine the limits of detection based on SWIR spectroscopy.

Several factors largely prevent the detection limits obtained from these binary mixture samples and the natural ones from being strictly equal. However, the limits presented in this study are the result of a systematic and simplified approach (i.e., only binary mixtures), carried out to illustrate a considerably more complex problem that is the identification of polymineralic natural samples using VNIR-SWIR spectroscopy. It is important to remark that calcite and dolomite have surprisingly high detection limits, and these worsen after the application of the second derivative of the spectra. That is, the identification is only reliable in binary mixture samples with high content in these minerals. In a study with natural samples or based on remote-sensing data, this problem could be aggravated, and the resulting spectra could be misinterpreted, underestimating the content of key minerals. A simple example of this could occur during the identification of marl-rich terrains, where the spectral signature could "ignore" the actual carbonate content, and lead to the identification of the rocks as strictly clay-rich.

According to the results obtained, the use of mixtures for the quantification of minerals faces several difficulties. Although it has been shown that D, S and D_2 vary with the abundance of each mineral in the binary samples, the extrapolation of these results to quantification studies in natural samples cannot be carried out directly. This is mainly due to the spectral variability of clay minerals, which can occur even within particular groups (such as kaolinites). The latter has been demonstrated in this study by observing not equal trends between mixtures of kaolinites with different crystallinities and, consequently, spectral responses. Differences between clay minerals, such as absorption coefficients or absorption bands, only make extrapolation of results

even more difficult. For example, the morphology, number, and position of bands (in the range between 2100 nm and 2500 nm) vary between members of the smectite group as they are strongly dependent on the octahedral cation composition. Despite these limitations, this quantification technique could be successfully implemented in more restricted case studies. An example of this application could be carried out for ore control purposes in mining. In this framework, with a good spectral characterization of the minerals extracted, mixtures sets would be prepared in advance and parameter-trendlines calculated, in order to estimate the mineral-content in samples provided from the mining face.

CRediT authorship contribution statement

Ángel Santamaría-López: Writing – review & editing, Writing – original draft, Visualization, Investigation, Formal analysis, Conceptualization. **Mercedes Suárez:** Writing – review & editing, Supervision, Methodology, Investigation, Funding acquisition, Conceptualization. **Emilia García-Romero:** Writing – review & editing, Funding acquisition.

Declaration of competing interest

The authors declare that they have no known competing financial interests or personal relationships that could have appeared to influence the work reported in this paper.

Data availability

Data will be made available on request.

Acknowledgements

The authors would like to express their gratitude to the reviewers and the editor for their constructive comments and suggestions. This study was supported by Junta de Castilla y León, Spain, and Fondo Europeo de Desarrollo Regional (FEDER) (grant number SA0107P20). We acknowledge the technical support provided by the "Servicio de preparación de rocas" of Universidad de Salamanca. E. Manchado is especially recognized for helping with the spectroradiometer data acquisition.

Appendix A. Supplementary data

Supplementary data to this article can be found online at https://doi.org/10.1016/j.clay.2024.107269.

References

Alayet, F., Mezned, N., Abdelaziz, S., Abdeljaouad, S., 2017. Continuum removed band depth analysis for carbonate mining waste quantification using X-ray diffraction and hyperspectral spectroscopy in the north of Tunisia. J. Appl. Remote. Sens. 11 (1), 016021 https://doi.org/10.1117/1.JRS.11.016021.

Bishop, J.L., 2019. Visible and near-infrared reflectance spectroscopy: laboratory spectra of geologic materials. In: Bishop, J., Bell III, J., Moersch, J. (Eds.), Remote Compositional Analysis: Techniques for Understanding Spectroscopy, Mineralogy, and Geochemistry of Planetary Surfaces. Cambridge University Press, Cambridge, pp. 68–101. https://doi.org/10.1017/9781316888872.006.

Bishop, J.L., Madejová, J., Komadel, P., Fröschl, H., 2002. The influence of structural Fe, Al and Mg on the infrared OH bands in spectra of dioctahedral smectites. Clay Miner. 37, 607–616. https://doi.org/10.1180/0009855023740063.

Bishop, J.L., Lane, M.D., Dyar, M.D., Brown, A.J., 2008. Reflectance and emission spectroscopy study of four groups of phyllosilicates: smectites, kaolinite-serpentines, chlorites and micas. Clay Miner. 43, 35–54. https://doi.org/10.1180/claymin.2008.043.1.03.

Bishop, J.L., Gates, W.P., Makarewicz, H.D., McKeown, N.K., Hiroi, T., 2011. Reflectance spectroscopy of beidellites and their importance for mars. Clay Clay Miner. 59, 378–399. https://doi.org/10.1346/CCMN.2011.0590403.

Bishop, J.L., Michalski, J.R., Carter, J., Gates, W.P., 2017. Remote detection of clay minerals. In: Kloprogge, J.T., Madejová, J., Bergaya, F. (Eds.), Developments in Clay Science. Elsevier, pp. 482–514. https://doi.org/10.1016/B978-0-08-100355-8.00014-X.

Bishop, J.L., King, S.J., Lane, M.D., Brown, A.J., Lafuente, B., Hiroi, T., Roberts, R., Swayze, G.A., Lin, J.F., Sánchez Román, M., 2021. Spectral properties of anhydrous carbonates and nitrates. Earth Space Sci. 8 (10) https://doi.org/10.1029/2021EA001844.

Bou-Orm, N., Al Romaithi, A.A., Elrmeithi, M., Ali, F.M., Nazzal, Y., Howari, F.M., Al Aydaroos, F., 2020. Advantages of first-derivative reflectance spectroscopy in the VNIR-SWIR for the quantification of olivine and hematite. Planet. Space Sci. 188 https://doi.org/10.1016/j.pss.2020.104957.

Cardoso-Fernandes, J., Silva, J., Rías, F., Lima, A., Teodoro, A.C., Barrès, O., Cauzid, J., Perrotta, M., Roda-Robles, E., Ribeiro, M.A., 2021. Tools for remote exploration: A lithium (Li) dedicated spectral library of the Fregeneda–Almendra aplite–pegmatite field. Data 6, 33. https://doi.org/10.3390/data6030033.

Çelik, M., Karakaya, N., Temel, A., 1999. Clay minerals in hydrothermally altered volcanic rocks, Eastern Pontides, Turkey. Clay Clay Miner. 47, 708–717. https://doi.org/10.1346/CCMN.1999.0470604.

Chipera, S.J., Bish, D.L., 2001. Baseline studies of the clay minerals society source clays: Powder X-ray diffraction analyses. Clay Clay Miner. 49, 398–409. https://doi.org/10.1346/CCMN.2001.0490507.

Clark, R.N., 1999. Chapter 1: Spectroscopy of rocks and minerals, and principles of spectroscopy. In: Rencz, N.A. (Ed.), Remote Sensing for the Earth Sciences: Manual of Remote Sensing. John Wiley & Sons, New York, pp. 3–58.

Clark, R.N., Roush, T.L., 1984. Reflectance spectroscopy: quantitative analysis techniques for remote sensing applications. J. Geophys. Res. 89, 6329–6340. https://doi.org/10.1029/JB089iB07p06329.

Clark, R.N., King, T.V.V., Klejwa, M., Swayze, G.A., Vergo, N., 1990. High spectral resolution reflectance spectroscopy of minerals. J. Geophys. Res. 95 (B8), 12653–12680. https://doi.org/10.1029/jb095ib08p12653.

Clark, R.N., Swayze, G.A., Livo, K.E., Kokaly, R.F., Sutley, S.J., Dalton, J.B., McDougal, R. R., Gent, C.A., 2003. Imaging spectroscopy: Earth and planetary remote sensing with the USGS Tetracorder and expert systems. J. Geophys. Res. 108 https://doi.org/10.1029/2002je001847.

Cloutis, E.A., Hawthorne, F.C., Mertzman, S.A., Krenn, K., Craig, M.A., Marcino, D., Methot, M., Strong, J., Mustard, J.F., Blaney, D.L., Bell, J.F., Vilas, F., 2006. Detection and discrimination of sulfate minerals using reflectance spectroscopy. Icarus 184 (1), 121–157. https://doi.org/10.1016/j.icarus.2006.04.003.

Cloutis, E.A., Grasby, S.E., Last, W.M., Léveillé, R., Osinski, G.R., Sherriff, B.L., 2010. Spectral reflectance properties of carbonates from terrestrial analogue environments: Implications for Mars. Planet. Space Sci. 58, 522–537. https://doi.org/10.1016/j.pss.2009.09.002.

Crowley, J.K., 1986. Visible and near-infrared spectra of carbonate rocks: Reflectance variations related to petrographic texture and impurities. J. Geophys. Res. 91, 5001–5012. https://doi.org/10.1029/jb091ib05p05001.

Delineau, T., Allard, T., Muller, J.P., Barres, O., Yvon, J., Cases, J.M., 1994. FTIR Reflectance vs. EPR studies of structural iron in kaolinites. Clay Clay Miner. 42 (3), 308–320. https://doi.org/10.1346/CCMN.1994.0420309.

Demetriades-Shah, T.H., Steven, M.D., Clark, J.A., 1990. High resolution derivative spectra in remote sensing. Remote Sens. Environ. 33, 55–64. https://doi.org/10.1016/0034-4257(90)90055-Q.

Desta, F., Buxton, M., 2020. Image and point data fusion for enhanced discrimination of ore and waste in mining. Minerals 10, 1110. https://doi.org/10.3390/min10121110.

Dill, H.G., 2016. Kaolin: soil, rock and ore from the mineral to the magmatic, sedimentary and metamorphic environment. Earth Sci. Rev. 161, 16–129. https://doi.org/10.1016/j.earscirev.2016.07.003.

Ducasse, E., Adeline, K., Briottet, X., Hohmann, A., Bourguignon, A., Grandjean, G., 2020. Montmorillonite estimation in clay-quartz-calcite samples from laboratory SWIR imaging spectroscopy: a comparative study of spectral preprocessings and unmixing methods. Remote Sens. 12, 1723. https://doi.org/10.3390/rs12111723.

Flahaut, J., Quantin, C., Clenet, H., Allemand, P., Mustard, J.F., Thomas, P., 2012. Pristine Noachian crust and key geologic transitions in the lower walls of Valles Marineris: Insights into early igneous processes on Mars. Icarus 221, 420–435. https://doi.org/10.1016/j.icarus.2011.12.027.

Gaffey, S.J., 1986. Spectral reflectance of carbonate minerals in the visible and near infrared (0.35-2.55 microns): calcite, aragonite, and dolomite. Am. Mineral. 71 (1–2), 151–162. https://doi.org/10.1029/JB092iB02p01429.

García-Rivas, J., Suárez, M., García-Romero, E., García-Meléndez, E., 2018. Identification and classification of mineralogical associations by VNIR-SWIR spectroscopy in the Tajo basin (Spain). Int. J. Appl. Earth Obs. Geoinf. 72, 57–65. https://doi.org/10.1016/j.jag.2018.05.028.

Géring, L., Kirsch, M., Thiele, S., De Lima Ribeiro, A., Gloaguen, R., Gutzmer, J., 2022. Spectral characterisation of hydrothermal alteration associated with sediment-hosted Cu-Ag mineralisation in the central European Kupferschiefer. Solid Earth 14, 463–484. https://doi.org/10.5194/egusphere-2022-825.

Gomez, C., Lagacherie, P., Coulouma, G., 2008. Continuum removal versus PLSR method for clay and calcium carbonate content estimation from laboratory and airborne hyperspectral measurements. Geoderma 148, 141–148. https://doi.org/10.1016/j.geoderma.2008.09.016.

Gomez, C., Drost, A.P.A., Roger, J.M., 2015. Analysis of the uncertainties affecting predictions of clay contents from VNIR/SWIR hyperspectral data. Remote Sens. Environ. 156, 58–70. https://doi.org/10.1016/j.rse.2014.09.032.

Gomez, C., Adeline, K., Bacha, S., Driessen, B., Gorretta, N., Lagacherie, P., Roger, J.M., Briottet, X., 2018. Sensitivity of clay content prediction to spectral configuration of VNIR/SWIR imaging data, from multispectral to hyperspectral scenarios. Remote Sens. Environ. 204, 18–30. https://doi.org/10.1016/j.rse.2017.10.047.

Haest, M., Cudahy, T., Laukamp, C., Gregory, S., 2012. Quantitative mineralogy from infrared spectroscopic data. I. Validation of mineral abundance and composition

scripts at the rocklea channel iron deposit in Western Australia. Econ. Geol. 107, 209–228. https://doi.org/10.2113/econgeo.107.2.209.
Hapke, B., 2002. Bidirectional reflectance spectroscopy. 5. The coherent backscatter opposition effect and anisotropic scattering. Icarus 157 (2), 523–534. https://doi.org/10.1006/icar.2002.6853.
Hubbard, B.E., Gallegos, T.J., Stengel, V., Hoefen, T.M., Kokaly, R.F., Elliott, B., 2024. Hyperspectral (VNIR-SWIR) analysis of roll front uranium host rocks and industrial minerals from Karnes and Live Oak Counties, Texas Coastal Plain. J. Geochem. Explor. 257, 107370 https://doi.org/10.1016/j.gexplo.2023.107370.
Hunt, G.R., 1977. Spectral signatures of particulate minerals in the visible and near infrared. Geophysics 42 (3), 501–513. https://doi.org/10.1190/1.1440721.
Kariuki, P.C., Woldai, T., van der Meer, F., 2004. Effectiveness of spectroscopy in identification of swelling indicator clay minerals. Int. J. Remote Sens. 25 (2), 455–469. https://doi.org/10.1080/0143116031000084314.
Lagacherie, P., Baret, F., Feret, J.B., Madeira Netto, J., Robbez-Masson, J.M., 2008. Estimation of soil clay and calcium carbonate using laboratory, field and airborne hyperspectral measurements. Remote Sens. Environ. 112, 825–835. https://doi.org/10.1016/j.rse.2007.06.014.
Madejová, J., Komadel, P., 2001. Baseline studies of the clay minerals society source clays: infrared methods. Clay Clay Miner. 49, 410–432. https://doi.org/10.1346/CCMN.2001.0490508.
Madejová, J., Gates, W.P., Petit, S., Gates, W.P., 2017. IR spectra of clay minerals. In: Kloprogge, J.T., Madejová, J., Bergaya, F. (Eds.), Developments in Clay Science. Elsevier, pp. 107–149. https://doi.org/10.1016/B978-0-08-100355-8.00005-9.
Makarewicz, H.D., Parente, M., Bishop, J.L., 2009. Deconvolution of VNIR spectra using modified Gaussian modeling (MGM) with automatic parameter initialization (API) applied to CRISM. In: WHISPERS '09 – 1st Workshop on Hyperspectral image and Signal Processing: Evolution in Remote Sensing Grenoble, France, 2009, pp. 1–5. https://doi.org/10.1109/WHISPERS.2009.5289046.
Mathian, M., Hebert, B., Baron, F., Petit, S., Lescuyer, J., Furic, R., Beaufort, D., 2018. Identifying the phyllosilicate minerals of hypogene ore deposits in lateritic saprolites using the near-IR spectroscopy second derivative methothology. J. Geochem. Explor. 186, 198–314. https://doi.org/10.1016/j.gexplo.2017.11.019.
McKeown, N.K., Bishop, J.L., Cuadros, J., Hillier, S., Amador, E., Makarewicz, H.D., Parente, M., Silver, E.A., 2011. Interpretation of reflectance spectra of clay mineral-silica mixtures: implications for Martian clay mineralogy at Mawrth Vallis. Clay Clay Miner. 59, 400–415. https://doi.org/10.1346/CCMN.2011.0590404.
Menges, F., 2016. Spectragryph-Optical Spectroscopy Software (Version 1.2.15). http://www.effemm2.de/spectragryph/.
Mulder, V.L., Plötze, M., de Bruin, S., Schaepman, M.E., Mavris, C., Kokaly, R.F., Egli, M., 2013. Quantifying mineral abundances of complex mixtures by coupling spectral deconvolution of SWIR spectra (2.1-2.4 μm) and regression tree analysis. Geoderma 207–208, 279–290. https://doi.org/10.1016/j.geoderma.2013.05.011.
Naimi, S., Ayoubi, S., Di Raimo, L.A.D.L., Dematte, J.A.M., 2022. Quantification of some intrinsic soil properties using proximal sensing in arid lands: application of Vis-NIR, MIR, and pXRF spectroscopy. Geoderma Reg. 28, e00484 https://doi.org/10.1016/j.geodrs.2022.e00484.
Ohiara, T.M., Taylor, K.G., Dowey, P.J., 2023. Mineral diagenesis in a carbonate-rich mudstone: the lower Carboniferous Hodder Mudstone, UK. Geol. Soc. Spec. Publ. 534 https://doi.org/10.1144/SP534-2021-42.
Pilorget, C., Fernando, J., 2021. Quantifying the minerals abundances on planetary surfaces using VIS-NIR spectroscopy, what uncertainties should we expect? General results and application to the case of phyllosilicates and carbonates on Mars. Icarus 365 (114498), 114498. https://doi.org/10.1016/j.icarus.2021.114498.
Pompilio, L., Pedrazzi, G., Sgavetti, M., Cloutis, E.A., Craig, M.A., Roush, T.L., 2009. Exponential Gaussian approach for spectral modeling: the EGO algorithm I. Band saturation. Icarus 201, 781–794. https://doi.org/10.1016/j.icarus.2009.01.022.
Poulet, F., Bibring, J.P., Mustard, J.F., Gendrin, A., Mangold, N., Langevin, Y., Arvidson, R.E., Gondet, B., Gomez, C., Berthe, M., Erard, S., Forni, O., Manaud, N., Poulleau, G., Soufflot, A., Combes, M., Drossart, P., Encrenaz, T., Fouchet, T., Melchiorri, R., Bellucci, G., Altieri, F., Formisano, V., Fonti, S., Capaccioni, F., Cerroni, P., Coradini, A., Korablev, O., Kottsov, V., Ignatiev, N., Titov, D., Zasova, L., Pinet, P., Schmitt, B., Sotin, C., Hauber, E., Hoffmann, H., Jaumann, R., Keller, U., Forget, F., 2005. Phyllosilicates on Mars and implications for early martian climate. Nature 438, 623–627. https://doi.org/10.1038/nature04274.
Ramanaidou, E.R., Wells, M., 2015. A new toolkit for iron ore characterization. Proc. Iron Ore 2015, 587–590. https://doi.org/10.1016/j.gexplo.2017.11.019.
Rialland, R., Soussen, C., Marion, R., Carrere, V., 2021. Improved deconvolution of mineral reflectance spectra. IEEE J Sel. Top. Appl. Earth Obs. Remote Sens. 14, 9711–9726. https://doi.org/10.1109/JSTARS.2021.3110008.
Robertson, K.M., Milliken, R.E., Li, S., 2016. Estimating mineral abundances of clay and gypsum mixtures using radiative transfer models applied to visible-near infrared reflectance spectra. Icarus 277, 171–186. https://doi.org/10.1016/j.icarus.2016.04.034.
Shkuratov, Y.G., Grynko, Y.S., 2005. Light scattering by media composed of semitransparent particles of different shapes in ray optics approximation: consequences for spectroscopy, photometry, and polarimetry of planetary regoliths. Icarus 173, 16–28. https://doi.org/10.1016/j.icarus.2003.12.022.
Shkuratov, Y.G., Kreslavsky, M.A., Ovcharenko, A.A., Stankevich, D.G., Zubko, E.S., Pieters, C., Arnold, G., 1999. Opposition effect from clementine data and mechanisms of backscatter. Icarus 141, 132–155. https://doi.org/10.1006/icar.1999.6154.
Simpson, M.P., 2015. Reflectance spectrometry (SWIR) of alteration minerals surrounding the Favona epithermal vein, Waihi vein system, Hauraki Goldfield. In: Proceedings of the Australasian Institute of Mining and Metallurgy New Zealand Branch Conference. Dunedin, pp. 409–418.
Simpson, M.P., Rae, A.J., 2018. Short-wave infrared (SWIR) reflectance spectrometric characterization of clays from geothermal systems of the Taupo Volcanic Zone, New Zealand. Geothermics 73, 74–90. https://doi.org/10.1016/j.geothermics.2018.01.006.
Sunshine, J.M., Pieters, C.M., 1993. Estimating modal abundances from the spectra of natural and laboratory pyroxene mixtures using the modified Gaussian Model. J. Geophys. Res. 98, 9075–9087.
Sunshine, J.M., Pieters, C.M., Pratt, S.F., 1990. Deconvolution of mineral absorption bands: an improved approach. J. Geophys. Res. 95, 6955–6966. https://doi.org/10.1029/JB095iB05p06955.
Tiecher, T., Moura-Bueno, J.M., Caner, L., Minella, J.P.G., Evrard, O., Ramon, R., Naibo, G., Barros, C.A.P., Silva, Y.J.A.B., Amorim, F.F., Rheinheimer, D.S., 2021. Improving the quantification of sediment source contributions using different mathematical models and spectral preprocessing techniques for individual or combined spectra of ultraviolet–visible, near- and middle-infrared spectroscopy. Geoderma 384, 114815. https://doi.org/10.1016/j.geoderma.2020.114815.
Warr, L.N., 2021. IMA–CNMNC approved mineral symbols. Mineral. Mag. 85, 291–320. https://doi.org/10.1180/mgm.2021.43.
Zhang, G., Wasyliuk, K., Pan, Y., 2001. The characterization and quantitative analysis of clay minerals in the Athabasca basin, Saskatchewan: application of shortwave infrared reflectance spectroscopy. Can. Mineral. 39 (5), 1347–1363. https://doi.org/10.2113/gscanmin.39.5.1347.